CHAPTER 2
THEORIES

2.1 Graphene and graphene oxide

Recently, graphene, as a two-dimensional of sp^2 carbon bonding network, has been of interest in photocatalyst applications because of its properties, Young's modulus of 1 TPa, tensile strength of 130 GPa, electron mobility 2×10^5 cm^2 $V^{-1}s^{-1}$ and high surface area 1850–2630 m^2 g^{-1} (Pan et al., 2011). Generally, graphene oxide was prepared from natural graphite and further converted to graphene by reduction processes such as hydrothermal method (Zhang et al., 2010a), chemical reduction (Dreyer et al., 2009) and UV-assisted photocatalytic reduction (Williams et al., 2008). In the case of graphene oxide, there are many chemical reagents that were used to synthesize graphene oxide.

There are many methods that were introduced to synthesize graphene oxide, such as Brodie's, Staudenmaier's and Hummer's methods. The aforementioned methods involve the oxidation process of graphite by using many chemical reagents. Brodie's method, potassium chlorate ($KClO_3$) and fuming nitric acid (HNO_3) are used to oxidize graphite. Staudenmaier's modified Brodie's method by adding chlorate over the course of the reaction and using concentrated sulfuric (H_2SO_4) acid instated of HNO_3. Hummers method used a mixture of potassium permanganate ($KMnO_4$) and H_2SO_4 as oxidizing agents for preparation graphene oxide. This method was usually used in many literatures because the reaction of $KMnO_4$ and H_2SO_4 leads a bimetallic heptoxide which is more reactive than monometallic tetraoxide. The formation of dimanganeseheptoxide (Mn_2O_7) in the present of H_2SO_4 can be explained by using the chemical reaction below (2.1)–(2.2) (Dreyer et al., 2009).

$$KMnO_4 + 3H_2SO_4 \longrightarrow K^+ + MnO_3^+ + H_3O^+ + 3HSO_4^- \quad (2.1)$$

$$MnO_3^+ + MnO_4^- \longrightarrow Mn_2O_7 \quad (2.2)$$

Tromel and Russ have suggested that the presence of Mn_2O_7 oxidise unsaturated aliphatic double bonds including any aromatic rings that exist in graphite. The structure of graphene oxide has been studied. However, the exact structure model of graphene oxide has not been observed because the complicated reaction of oxidation process and the complexity of

graphene oxide. Previous structural models of graphene oxide were introduced based on the stoichiometric principle. Hofmann and Holst suggested that the oxidation of graphite leads to an epoxy groups spread on the basal structure of graphene oxide. Scholz and Boehm introduced a new structural model of graphene oxide, which consists of quinoidal species in corrugated backbone. For Ruess's model, the basal carbon structure of graphene oxide should be presented in the form of sp^3 hybridized system as shown in Figure 2.1. The different structures of graphene oxide that were proposed by previous researches may due to a stepwise mechanism. Recently, the most well-known model of graphene oxide structure bases on non-stoichiometry was proposed by Lerf and Klinowaki (Dreyer et al., 2009). The structure of grapheme in Lerf–Klinowski model consists of epoxide (cyclic ether), hydroxyl (–OH) and carboxyl (–COOH) groups on the basal plane of graphene oxide as shown in Figure 2.2. Each of the functional group can be observed by using FTIR (He et al., 1996 and Szabo et al., 2006).

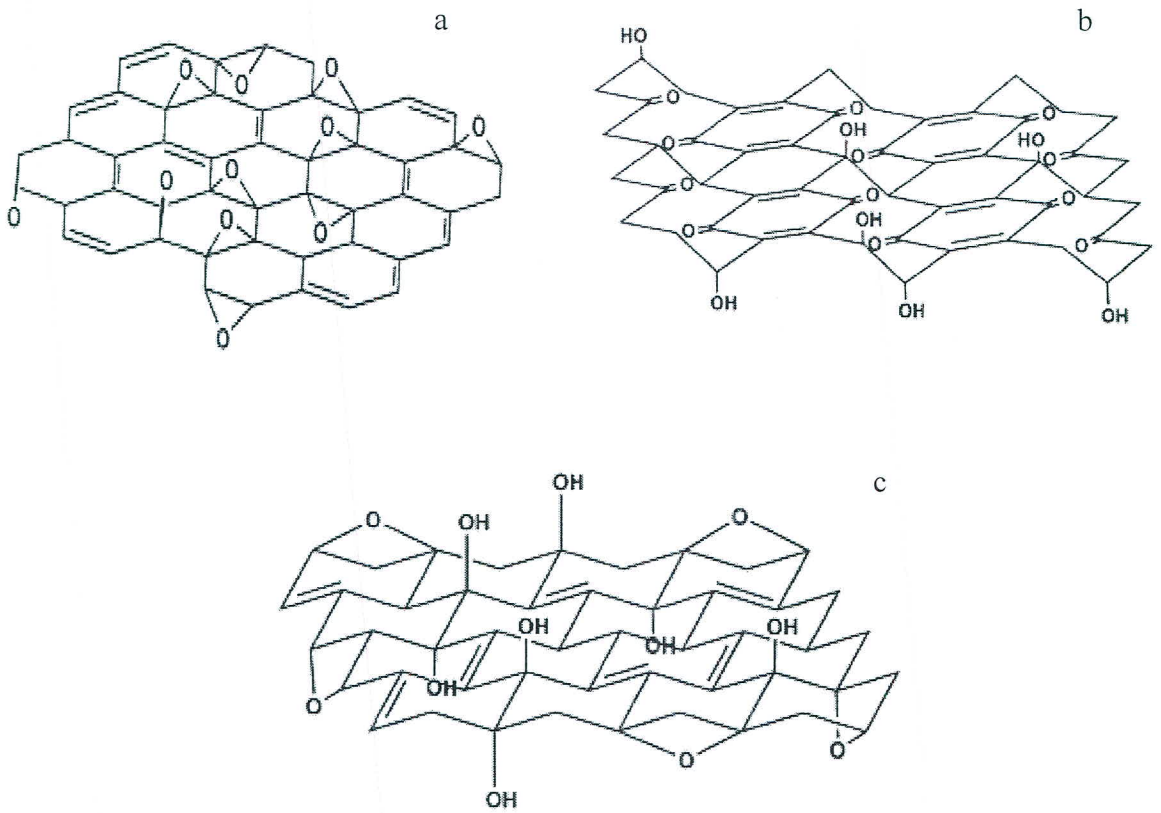

Figure 2.1 Possible structures of graphene oxide (a) Hofmann, (b) Scholz–Boehm and (c) Ruess models (Dreyer et al., 2009).

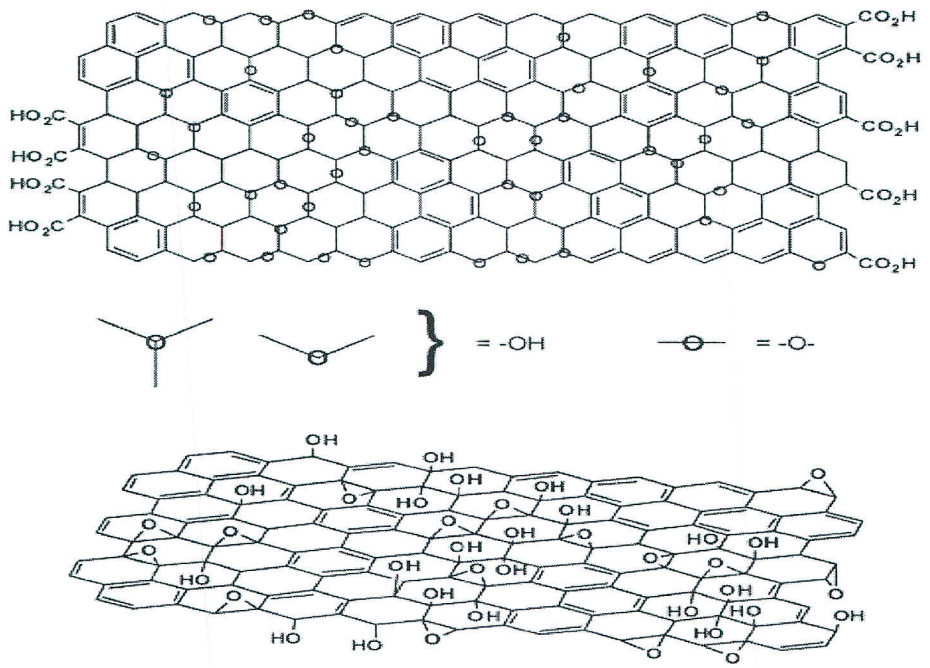

Figure 2.2 Possible structure of graphene oxide that was proposed by Lerf–Klinowski (Dreyer et al., 2009).

Graphene oxide is an electrically insulating material because of imperfect sp^2 carbon bonding network. In order to achieve the electrical conductivity, imperfect sp^2 carbon bonding network needs to be restored to perfect sp^2 carbon boning via reduction processes. Hydrazine monohydrate ($NH_2NH_2 \cdot H_2O$) is the first chemical regent that used to reduce graphene oxide to graphene. Stankovich et al. (2007) proposed the reaction pathway of epoxide reduction by hydrazine as shown in Figure 2.3.

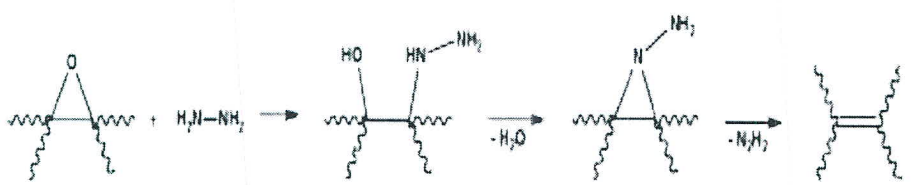

Figure 2.3 Reaction pathway of epoxide reduction by hydrazine (Stankovich et al., 2007).

After the reduction process, the graphene oxide is converted to graphene. In case of strong reducing agents, such as lithium aluminium hydride ($LiAlH_4$), the reduction pathway of reduced graphene oxide may be different from the mechanism of hydrazine because of the

side reaction of solvent (Paredes et al., 2008 and Novoselov et al., 2004). Mcallister et al. (2007) introduced the thermally–mediated reduction method using high temperature at 1050 °C to convert graphene oxide to graphene and stacked structure of graphene oxide is also exfoliated during this process. Stacked structure of graphene can also separate by sonication and/or mechanical stirring into monolayer or few–layered stacks of graphene (Pan et al., 2011). However, the mechanism of thermally–mediated reduction of graphene oxide has not reported. Graphene oxide can easily turn to graphene via the reactions of TiO_2 and ethyl alcohol (C_2H_5OH) under UV irradiation as shown in Equations (2.3)–(2.5).

$$TiO_2 + h\nu \longrightarrow TiO_2\,(h^+ + e^-) \quad (2.3)$$

$$TiO_2\,(h^+) + C_2H_5OH \longrightarrow {}^{\bullet}C_2H_4OH + H^+ \quad (2.4)$$

$$TiO_2\,(e^-) + \text{graphene oxide} \longrightarrow TiO_2 + \text{graphene} \quad (2.5)$$

TiO_2 (h^+) reacts with C_2H_5OH to produce ethoxy radical (${}^{\bullet}C_2H_4OH$) and TiO_2 (e^-) reacts with organic functional groups on the basal plane of graphene oxide (Williams et al., 2008).

2.2 Effect of graphene on TiO_2 photocatalyst

In previous reports, GR–TiO_2 exhibited the higher photocatalytic activities than that of TiO_2. The enhanced photocatalytic activity of TiO_2 by adding graphene can be described as follows: enhanced adsorptivity, extendable light absorption and increased charge separation and transportation.

Enhanced TiO_2 adsorptivity

According to the P25–graphene composite as a high performance photocatalyst report, the adsorption property of P25–graphene is higher than that of P25 because of large surface area of graphene. The sp^2 carbon network of graphene plays a vital role to adsorb methylene blue molecules on the surface of graphene using the interaction of π–π conjugated system between methylene blue and graphene. Contaminated organic molecules can be adsorbed on surface of graphene using noncovalent bond with offset face–to–face orientation of π–π conjugated system until adsorption-desorption equilibrium is reached (Zhang et al., 2010a and Yoo et al., 2011). Under UV or visible light irradiation,

the absorbed organic molecules are further degraded by high oxidative species such as hydroxyl and super oxide radicals.

Extendable light absorption

The results from UV–vis spectra showed that the absorption edge of GR–TiO_2 photocatalysts shift to longer wavelength (red shift) of 30–40 nm in comparison with that of TiO_2. Zhang et al. (2010b) estimated band gap of GR–TiO_2 by using Kubelka–Munk function. The estimated band gap of GR–TiO_2 from Zhang's work is 2.83, 3.02, 2.96, 3.17, 3.16, 3.19, 3.15 and 3.36 eV corresponding to graphene 30, 10, 5, 2, 1, 0.5, 0.2 wt% and bare P25, respectively.

Increased charge separation and transportation

When graphene oxide is turned to graphene, imperfect sp^2 bonding network is restored to complete π–π conjugation system. Therefore, graphene can act as the electron acceptor and transporter. The excited electrons from the valence band of TiO_2 transport to graphene base. In this case, graphene suppresses charge recombination of electrons–hole pairs of TiO_2. Thus, the electrons move and promote the degradation of organic molecules that are adsorbed on graphene basal (Zhang et al., 2010a).

2.3 Titanium dioxide (TiO_2) photocatalyst and its photocatalytic activity

The structure of titanium dioxide is composed of rutile, anatase and brookite. Rutile, anatase and brookite are not only different crystal structures but also changed lattice parameters, density and band gap energy and thermal stabilities (University of Colorado, 2011). Rutile phase can be synthesized at high temperature compared to anatase phase. In the case of brookite, it appears as an intermediate structure in the process of rutile to anatase phase transformation. Two different crystal structures of rutile and anatase are commonly used in photocatalysis but anatase structure shows a higher photocatalytic activity than that of rutile because of the high surface area of anatase. Ti^{4+} and O^{2-} ions bond with the appropriate positions in the form of TiO_6 octahedral structure. However, incomplete fill of Ti^{4+} and O^{2-} leads to defect on TiO_2 surface. The defect sites were found as the active sites for photocatalytic reaction. The defect sites can be divided into three

types, lattice vacancy, single bridging vacancy and double bridging vacancy (Linsebigler et al., 1995). The adsorption of H_2O and oxygen (O_2) on the surface of TiO_2 is an essential process for producing $^{\bullet}OH$ and $^{\bullet}O_2^-$ radicals. In fact, surface defect coverage was found to slight increase during water adsorption. This mechanism was proposed that an adsorbed water molecule reacts with a bridging-oxygen atom to form OH group (Kurtz et la., 1989) and it was also found that water molecules can be reduced at the Ti^{3+} sites on TiO_2 surface to produce hydrogen gas (Lu et la., 1994). Organic pollutants adsorbed on the surface of TiO_2 are oxidized by photooxidation process. Photooxidation occurs when catalyst absorbs light that has energy enough to excite electrons from the valence band to the conduction band of TiO_2. The structure of the energy level of TiO_2 can be roughly presented in Figure 2.4 (The Photochemistry Portal, 2009).

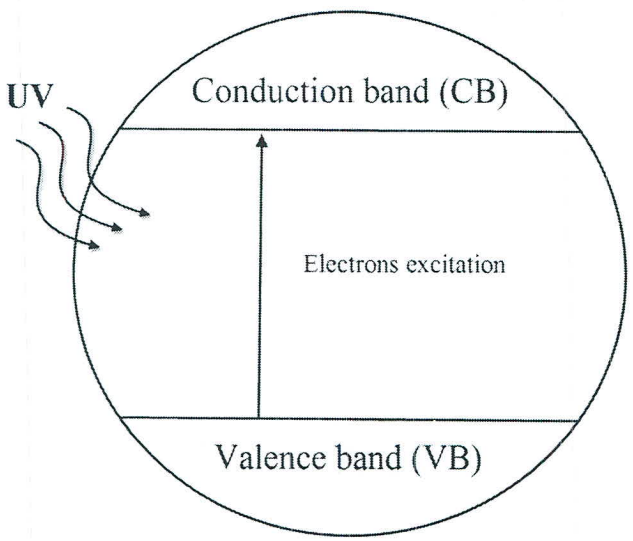

Figure 2.4 Schematic band gap structure and photoexcitation of TiO_2 photocatalyst.

The theoretical band gap energy of TiO_2 is approximately around 3.20 eV. The excited electrons from the valence band of TiO2 migrate and accumulate in the conduction band of TiO_2. The generation of electron–hole pairs under the photoexcitation by using UV light can be alternatively explained via Equation (2.6).

$$TiO_2 \longleftrightarrow TiO_2(e_{cb}^-) + TiO_2(h_{vb}^+) \quad (2.6)$$

Where cb is a conduction band and vb is a valence band.

The oxidation reaction of H_2O occurs at the conduction band of TiO_2 to produce $^{\bullet}OH$ radicals. For the valence band, O_2 molecules act as accepter molecules and are converted to $^{\bullet}O_2^-$ radicals. The fundamental processes of photocatalytic reaction were presented in Equation (2.7)–(2.10). The holes are trapped by H_2O molecules and react with Ti^{4+} at defect sites of TiO_2 to form OH groups on TiO_2 surface (Linsebigler et al., 1995).

$$Ti^{4+}–H_2O + h^+ \longleftrightarrow Ti^{4+}---^{\bullet}OH + H^+ \quad (2.7)$$

$$Ti^{4+}–OH + h^+ \longleftrightarrow Ti^{4+}---^{\bullet}OH \quad (2.8)$$

(--- means that the $^{\bullet}OH$ radical is associated with the Ti^{4+} site.)

The electrons in the conduction band are trapped at the surface of titanium dioxide by Ti^{4+} sites that further convert to Ti^{3+} sites. O_2 molecules react with Ti^{3+} resulting in the formation of superoxide radicals as shown in Equations 2.9–2.10.

$$Ti^{4+} + e^- \longleftrightarrow Ti^{3+} \quad (2.9)$$

$$Ti^{3+} + O_2 \longleftrightarrow Ti^{4+}---O_2^- \quad (2.10)$$

Organic pollutant molecules adsorbed on the surface of TiO_2 were further degraded to other molecular structures or completely converted to CO_2 and H_2O (Matthews et al., 1992; Draper et al., 1990 and Turchi et al., 1989, 1990). However, the degradation mechanism of organic compounds is quite difficult to explain by using simple chemical reactions. The degradation pathway of HCHO has been studied as shown in Equations (2.11)–(2.21). Formic acid is found as intermediate organic molecules in HCHO degradation pathway. In addition, the degradation rate of HCHO on TiO_2 photocatalyst may decrease because of the formation of formic acid (Lee et al., 2004).

$$CH_2O + h\nu \longrightarrow H + HCO^{\bullet} \quad (2.11)$$

$$^{\bullet}CHO + HO_2^{\bullet} \longrightarrow HOCH_2OO \quad (2.12)$$

$$HOCH_2OO + HO_2^{\bullet} \longrightarrow HOOCH_2OH + O_2 \quad (2.13)$$

$$HOOCH_2OH \longrightarrow H_2O + HCOOH \quad (2.14)$$

$$TiO_2 + h\nu \longrightarrow TiO_2\,(e^-) + TiO_2\,(h^+) \quad (2.15)$$

$$H_2O \longrightarrow H^+ + OH^- \quad (2.16)$$

$$h^+ + OH^- \longrightarrow {}^{\bullet}OH \quad (2.17)$$

$$e^- + O_2 \longrightarrow O_2^- \quad (2.18)$$

$$HCHO + {}^{\bullet}OH \longrightarrow HCO^{\bullet} + H_2O \quad (2.19)$$

$$HCO^{\bullet} + {}^{\bullet}OH \longrightarrow HCOOH \quad (2.20)$$

$$HCOOH + 2h^+ \longrightarrow CO_2 + 2H^+ \quad (2.21)$$

In the case of MB degradation, the degradation pathway of MB is different from HCHO because of the complicated molecular structure of MB as shown in Figure 2.5.

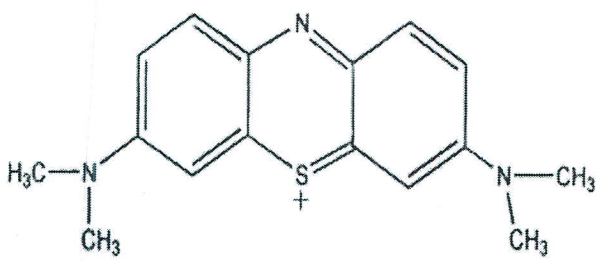

Figure 2.5 Molecular structure of methylene blue (Houas et. al., 2001).

The photocatalytic degradation pathway of MB in water was analyzed by Gas Chromatography-Mass Spectrometry (GC/MS) and Liquid Chromatography–Mass spectrometry (LC/MS) technique to identify types and fractions of ions that are generated from the MB degradation reaction. The oxidation of water by holes and transient formation of hydroperoxyl ($HO_2^{\bullet}$) radicals are two main processes to generate $^{\bullet}OH$ radicals and these reactions can be explained by the following reactions (Houas et al., 2001)

Oxidation of water by holes:

$$(H_2O \longrightarrow H^+ + OH^-) + h^+ \longrightarrow H^+ + {}^{\bullet}OH \quad (2.22)$$

Transient formation of hydroperoxyl radicals:

$$O_2\,(g) + e^- \longrightarrow O_2^- \quad (2.23)$$

$$O_2^- + H^+ \longrightarrow HO_2^{\bullet} \quad (2.24)$$

$$2HO_2^{\bullet} \longrightarrow H_2O_2 + O_2 \quad (2.25)$$

$$H_2O_2 + e^- \longrightarrow OH^- + {}^{\bullet}OH \quad (2.26)$$

It was obvious that the initial rate of MB degradation depends on the cleavage of the bonds C–S^+=C functional group in MB to sulfoxide (–S(=O)–) group on the surface titanium dioxide as shown in Figure 2.6.

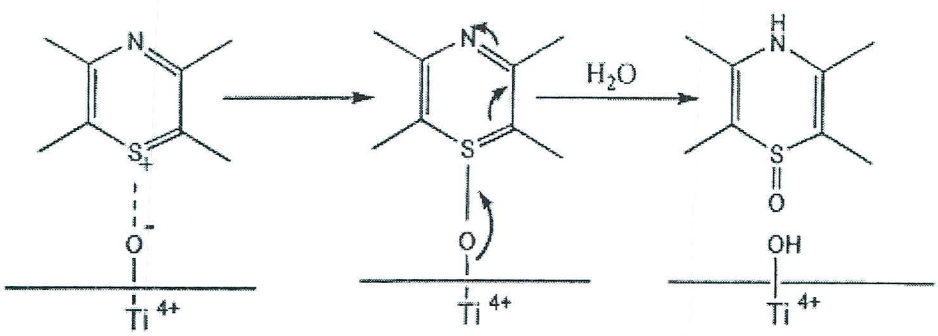

Figure 2.6 Cleavage of C–S^+=C bond in methylene blue to sulfoxide group (Houas et al., 2001).

The sulfoxide group can undergo a reaction with ${}^{\bullet}OH$ radical and is further converted to sulfone (–$S(=O)_2$–) group via dissociation of the two benzene rings (Equations (2.27) and (2.28)).

$$NH_2–C_6H_3(R)–(S=O)–C_6H_4–R + {}^{\bullet}OH \longrightarrow NH_2–C_6H_3(R)–SO_2 + C_6H_5–R \quad (2.27)$$

$$NH_2–C_6H_3(R)–(S=O)–C_6H_4–R + {}^{\bullet}OH \longrightarrow NH_2–C_6H_4–R + SO_2–C_6H_4–R \quad (2.28)$$

There are many intermediate molecules that observed in the MB degradation pathway as shown in Figure 2.7.

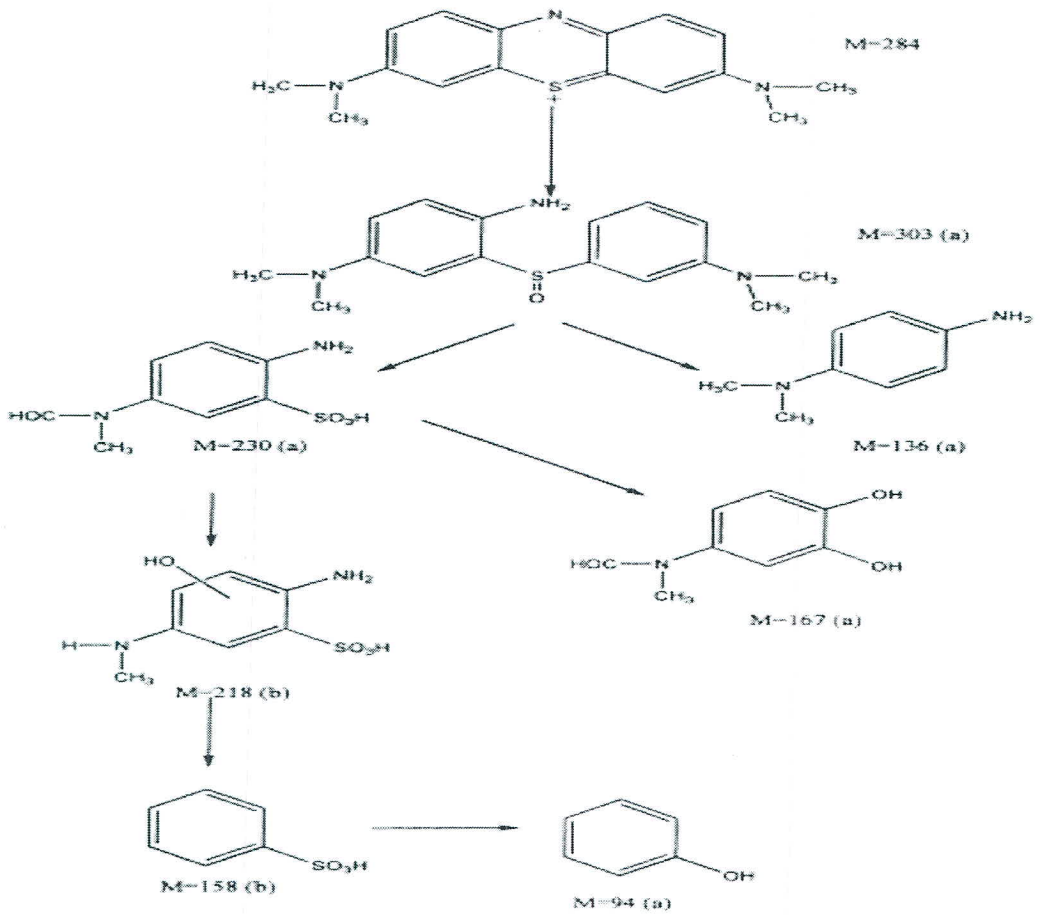

Figure 2.7 Photocatalytic degradation pathway of methylene blue (Houas et al., 2001). (Where a is the mass of fraction ions that were detected by GC/MS and b is the mass of fraction ions that were detected by LC/MS)

Briefly, when a central aromatic ring in MB is opened, it will undergo hydroxylation producing phenyl molecule. The amino group can convert to ammonium ions that are slowly oxidized to nitrate (Fu et al., 2008).

2.4 Effect of metal and nonmetal doped TiO_2

TiO_2 has a band gap energy of about 3.2 eV. Therefore, the need of UV light as a source for TiO_2 photoexcitation limits its applications. The strategies that are used to enhance photocatalytic activity of TiO_2 can be divided into two major types, doping and surface chemical modification. Doping, metal and nonmetal ions are used to modify band gap of

TiO_2. Lower band gap energy of metal or nonmetal–TiO_2 is the cause of the absorption of photoresponse in visible light region. Chen and Mao (2007) reported that the electronic state of TiO_2 can be separated into three paths:

- The σ bonding of the oxygen atom (p_σ) and Ti e_g states in the valence band region
- The π bonding of O p_π and Ti t_{2g} states in the lower conduction band region
- The bonding between O p_σ and Ti e_g states in the upper conduction band

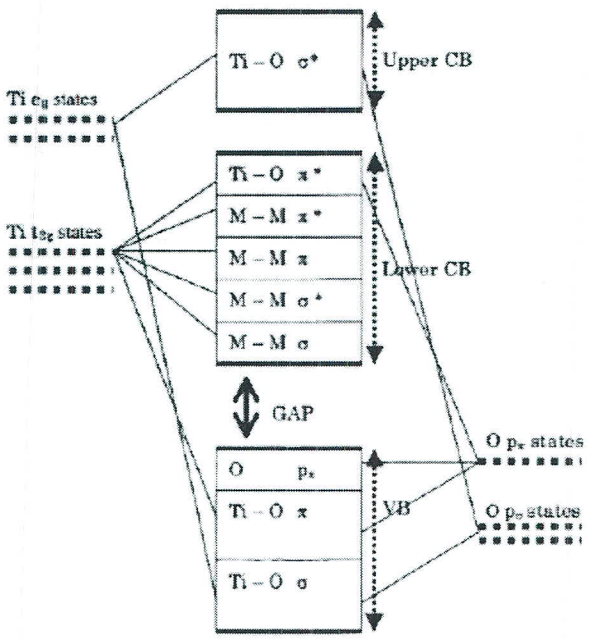

Figure 2.8 Bonding diagram of TiO_2 (Chen and Mao, 2007).

In the case of metal-doped modification, the electronic state of TiO_2 can be shifted to lower energy levels because the metal dopant can generate a new electron-occupied level form. A new electron occupier level may lie at the top of the valence band or below the conduction band of TiO_2. In consequence of the decrease in band gap energy level of metal-doped TiO_2, the photoexcitation reaction of metal-doped TiO_2 can easily occurs under visible light irradiation and red shift in absorption edge of metal-doped TiO_2 was observed. According to the Wonyong et al. (1994) report's, the increase in photooxidation of metal ions doped TiO_2 can be deeply explained by consideration the acting of metal ions in photoexcitation process. Metal ions can act as an electron or hole traps when the energy level of $M^{n+}/M^{(n-1)+}$ lies below the conduction band of TiO_2 and it plays a vital role for prevention electron-hole pairs recombination as shown in Equations (2.29) and (2.30).

$$M^{n+} + e_{cb}^{-} \longrightarrow M^{(n-1)+} \text{ electron trap} \quad (2.29)$$

$$M^{n+} + h_{vb}^{+} \longrightarrow M^{(n+1)+} \text{ hole trap} \quad (2.30)$$

The energy of metal ion impurities in rutile TiO_2 was introduced by Mizushima et al. (1979) and Triggs et al. (1985) as show in Figure 2.9.

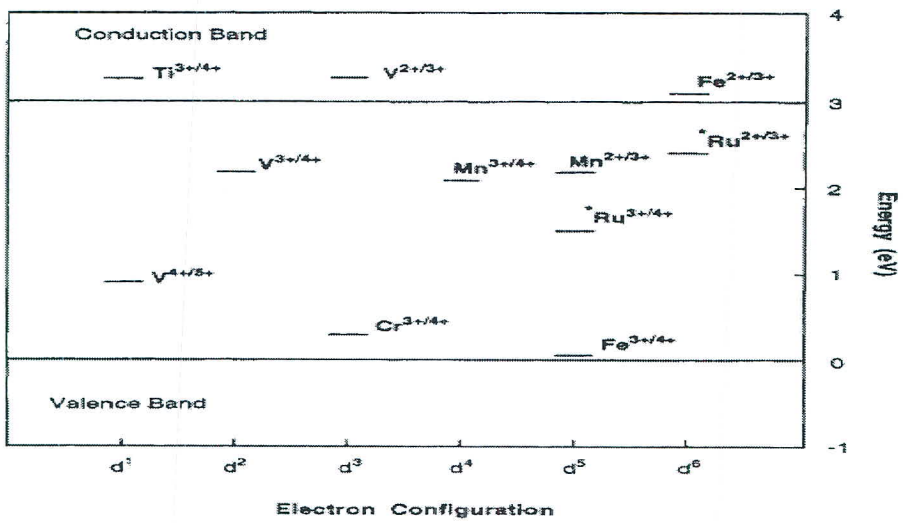

Figure 2.9 Energy levels of impurity ions in TiO_2 photocatalyst (Mizushima et al., 1979 and Triggs et al., 1985).

Therefore, the band gap energy of TiO_2 can be reduced by adding transition ions. Furthermore, interfacial charge transfer, charge pair generation, charge trapping, charge release, migration and recombination, which are explained by the increase in photocatalytic activity of the metal doped TiO_2 photocatalyst, was introduced by Mizushima et al. (1979) and Triggs et al. (1985) as shown in Equations (2.31)–(2.47).

Charge pair generation

$$TiO_2 + h\nu \longrightarrow TiO_2\,(e_{cb}^{-}) + TiO_2\,(h_{vb}^{+}) \quad (2.31)$$

$$M^{n+} + h\nu \longrightarrow M^{(n+1)+} + e_{cb}^{-} \quad (2.32)$$

$$M^{n+} + h\nu \longrightarrow M^{(n-1)+} + h_{vb}^{+} \quad (2.33)$$

Charge trapping

$$Ti^{4+} + e_{cb}^{-} \longrightarrow Ti^{3+} \quad (2.34)$$

$$M^{n+} + e_{cb}^{-} \longrightarrow M^{(n-1)+} \quad (2.35)$$

$$M^{n+} + h_{vb}^{+} \longrightarrow M^{(n+1)+} \quad (2.36)$$

$$OH^- + h_{vb}^+ \longrightarrow {}^{\bullet}OH \quad (2.37)$$

Charge release and migration

$$M^{(n-1)+} + Ti^{4+} \longrightarrow M^{n+} + Ti^{3+} \quad (2.38)$$

$$M^{(n+1)+} + >OH^- \longrightarrow M^{n+} + >{}^{\bullet}OH \quad (2.39)$$

Recombination

$$TiO_2\,(e_{cb}^-) + TiO_2\,(h_{vb}^+) \longrightarrow TiO_2 \quad (2.40)$$

$$Ti^{3+} + {}^{\bullet}OH \longrightarrow Ti^{4+} + OH^- \quad (2.41)$$

$$M^{(n-1)+} + h_{vb}^+ \longrightarrow M^{n+} \quad (2.42)$$

$$M^{(n-1)+} + {}^{\bullet}OH \longrightarrow M^{n+} \quad (2.43)$$

$$M^{(n+1)+} + e_{cb}^- \longrightarrow M^{n+} \quad (2.44)$$

$$M^{(n+1)+} + Ti^{3+} \longrightarrow M^{n+} \quad (2.45)$$

Interfacial charge transfer

$$e_{cb}^-\ (\text{or } Ti^{3+}, M^{(n-1)+}) + O \longrightarrow O^- \quad (2.46)$$

$$h_{vb}^+\ (\text{or } >{}^{\bullet}OH, M^{(n+1)+}) + R \longrightarrow R^+ \quad (2.47)$$

Where M is a metal ion dopant, O is an electron acceptor, R is an electron donor. $> OH^-$ and $>{}^{\bullet}OH$ are trap sites for holes in addition to the surface trap sites. The effect of Fe^{3+} dopant on Fe^{3+}– TiO_2 photocatalyst was introduced by Zhu et al. (2006). When Fe^{3+}– TiO_2 was irradiated with UV or visible light, Fe^{3+} ion dopant gains electron from the conduction band of TiO_2. This process can prevent recombination of e_{cb}^- and h_{vb}^+ by using the following equations.

$$Fe^{3+} + e_{cb}^- \longrightarrow Fe^{2+} \quad (2.48)$$

$$Fe^{2+} + Ti^{4+} \longrightarrow Fe^{3+} + Ti^{3+} \quad (2.49)$$

$$Fe^{3+} + h^+ \longrightarrow Fe^{4+} \quad (2.50)$$

$$Fe^{4+} + e^- \longrightarrow Fe^{3+} \quad (2.51)$$

$$Fe^{2+} + h^+ \longrightarrow Fe^{3+} \quad (2.52)$$

Fe^{3+} is stable in comparison with that of Fe^{2+} because Fe^{3+} has half-filled d orbital (d^5). Therefore, electron from Fe^{2+} transfers to a neighboring surface Ti^{4+} and reacts with oxygen molecule to produce ${}^{\bullet}O_2^-$ radicals.

$$Fe^{2+} + O_2 \longrightarrow Fe^{3+} + {}^{\bullet}O_2^- \quad (2.53)$$

Figure 2.10 shows the possible mechanism of Fe^{3+}–TiO_2 that was proposed by Kaewtip et al. (2012c).

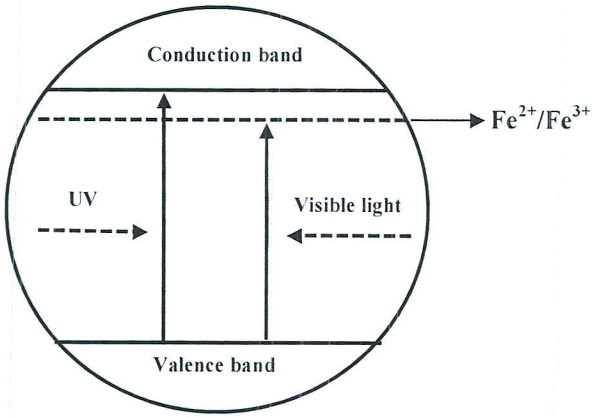

Figure 2.10 Possible mechanism of Fe^{3+}–TiO_2 photoexcitation (Kaewtip et al., 2012c).

Nonmetal dopants such as C, N and S can also be used to reduce band gap narrowing of TiO_2 by generating new energy level upper the conduction band of TiO_2. Nakano et al. (2005) found that C-doped TiO_2 introduces three deep energy levels at 0.86, 1.30 and 2.34 eV. However, energy level with 3.24 eV plays a vital role to band gap narrowing TiO_2 by mixing with the O 2p valence band. In the case of N-doped TiO_2, the band gap narrowing TiO_2 is the result of the mixing of N 2p states and O 2p states below the conduction band of TiO_2. It was found that there have two deep levels located at 1.18 and 2.48 eV below the conduction band that contribute to band gap narrowing by mixing with the O 2p valence band. S dopant gives a similar result as nitrogen. The mixing of sulfur 3p state with the valence band of TiO_2 is the cause of the thicker width of the valence band, leading to narrowing of the band gap (Chen and Mao. 2007). Wu et al. (2010) proposed a possible mechanism of iron and carbon co-doped TiO_2 as illustrated in Figure 2.11.

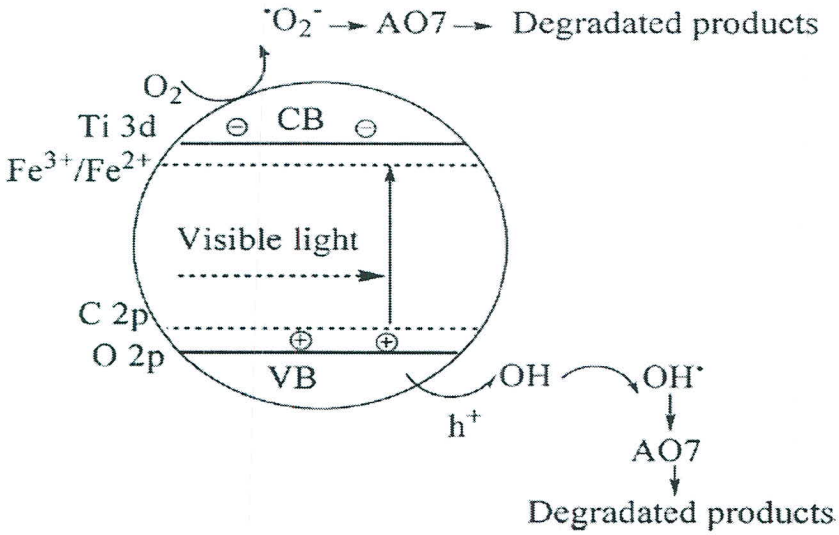

Figure 2.11 Synergistic effects of iron and carbon dopants on TiO_2 photoexcitation system (Wu et al., 2010).

The C 2p state of carbon lead an intra–band–gap energy level close to the valence band edges of the valence band of TiO_2 and substation positions of Fe^{3+} ions into the lattice of TiO_2 can introduce a new energy level below the conduction band of TiO_2, leading to the narrowing of the band gap of TiO_2. Under visible light irradiation, partial electrons from the valence band were trapped by Fe^{2+} ions. Subsequently, Fe^{2+} ions convert to Fe^{3+} and further react to absorb O_2 on the surface of TiO_2. Therefore, the recombination of electron–hole pairs is suppressed. Iron and carbon co-doped TiO_2 may not only improve the photocatalytic activity under visible light region by narrowing band gap of TiO_2, but also promote by interfacial charge transfer and charge trapping process (Wu et al., 2010).

2.5 Composite semiconductor

Composite semiconductor–semiconductor photocatalyst proved to be an effective route to improve the photocatalytic activity of TiO_2 photocatalyst by increase in the photoresponse under visible light irradiation. The proposed mechanisms of semiconductor–semiconductor photocatalyst base on the transmission excited electrons from narrow band gap semiconductor to another high band gap semiconductor as shown in Figure 2.12.

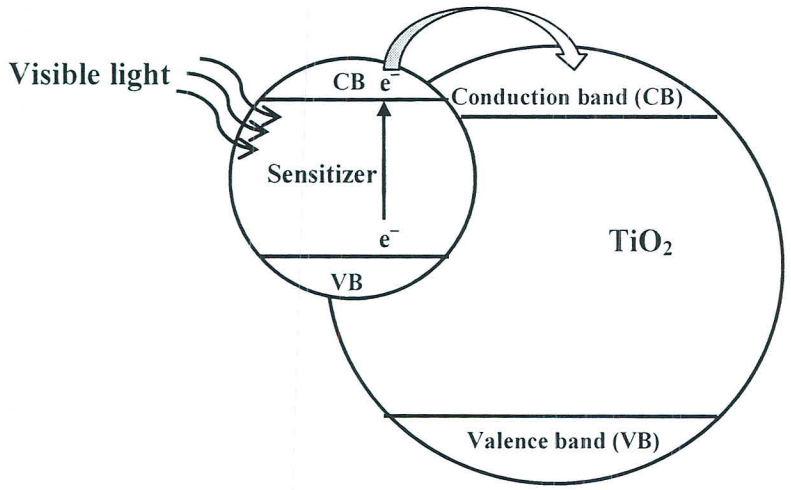

Figure 2.12 General concept of composite (coupled) semiconductor–semiconductor photocatalyst.

Linsebigler et al. (1995) explained the mechanism of the photoexcitation process for the composite (coupled) semiconductor-semiconductor photocatalyst CdS–TiO_2. In this system, the energy of visible light is large enough to excite an electron from the valence band to the conduction band of CdS (2.5 eV). The excited electrons transfers to the conduction band of TiO_2 but holes still remain in the CdS. In this case, CdS not only enhances the photoresponse under visible light region but also increases charge separation process. The separated hole and electron can undergo to react with adsorbed molecules on the surface of TiO_2 to produce more $^{\bullet}OH$ and $^{\bullet}O_2^-$ radicals.

Weller et al. (1994) reported the bang gap energy of Ag_2S about 1.3 eV. In Xei et al. (2010) report's, the band gap energy of Ag_2S was reported to be about 1.0 eV and the visible-light-induced catalytic activity of Ag_2S was completely proved by using UV-vis spectroscopy. The results show that Ag_2S-coupled TiO_2 nanoparticles show good absorption in visible light region. This report suggested that at the wavelength less than 387 nm was the absorption of anatase TiO_2 and the broad absorption in the visible region was the effect from Ag_2S coupling. Zhu et al. (2012a) and Shen et al., (2013) proposed the possible scheme of the photoexcitation including charge transfer process of Ag_2S–TiO_2 photocatalyst as shown in Figure 2.13.

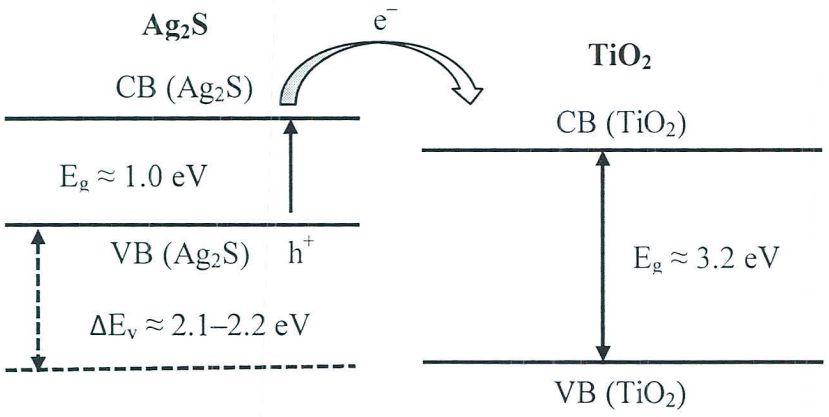

Figure 2.13 Band gap energy diagram and photoexcitation of Ag_2S–TiO_2 (Zhu et al., 2012a and Shen et al., 2013).

Under visible light irradiation, excited electrons from the valence band of Ag_2S migrate to the conduction band of TiO_2. The electron–hole pairs generation in Ag_2S–TiO_2 photocatalyst reacts with H_2O and O_2 to produce $^{\bullet}OH$ and $^{\bullet}O_2^-$ radicals as shown in Equations (2.54)–(2.58) (Zhu et al., 2012a).

$$Ag_2S + h\nu \longrightarrow Ag_2S\,(h^+) + Ag_2S\,(e^-) \quad (2.54)$$

$$Ag_2S\,(h^+, e^-)\text{–}TiO_2 \longrightarrow Ag_2S\,(h^+) + TiO_2\,(e^-) \quad (2.55)$$

$$e^- + O_2 \longrightarrow {}^{\bullet}O_2^- \quad (2.56)$$

$$h^+ + OH^- \longrightarrow {}^{\bullet}OH \quad (2.57)$$

$$h^+ + H_2O \longrightarrow {}^{\bullet}OH + H^+ \quad (2.58)$$

2.6 Silver sulfide (Ag_2S) preparation

Ag_2S is one of the narrow band gap semiconductors that can enhance the photoresponse of Ag_2S–TiO_2 by extending absorption to visible light region. Banerjee et al. (2007) synthesized Ag_2S nanocomposites using $AgNO_3$ and thiourea as precursors. In this method, thiourea was hydrolyzed to produce H_2S in hot alkaline medium and reacts with $AgNO_3$ to produce Ag_2S.

$$(NH_2)_2CS + 2H_2O \longrightarrow 2NH_3 + H_2S + CO_2 \quad (2.59)$$

$$H_2S + 2AgNO_3 \longrightarrow Ag_2S + 2HNO_3 \quad (2.60)$$

Xei et al. (2010) used silver acetate and thiourea for preparing Ag_2S under mild conditions without adding alkaline medium. This reaction can be used to synthesize Ag_2S-coupled TiO_2 nanoparticles by adding the solution of silver acetate and thiourea to PTA and refluxing at 98 °C for 6 h.

$$2CH_2COOAg + (NH_2)_2CS + 2H_2O \longrightarrow Ag_2S + 2NH_3 + CO_2 + 2CH_3COOH \quad (2.61)$$

The XRD pattern of Ag_2S prepared via chemical Equations (2.59)–(2.61) show diffraction peaks at 28.9°, 31.5°, 33.6°, 34.4°, 36.8°, 40.7° and 43.4° that was exactly matched with the acanthite Ag_2S phase (α–Ag_2S, JCPDS:14–0072).

2.7 Formation of peroxo titanic acid (PTA) and TiO_2

Inorganic salt and metal alkoxide are normally used as a starting material for preparation metal oxides. Metal alkoxide (ROM) is the organometallic compounds that the central metal ion binds with organic molecule(s). In other word, metal alkoxide can be explained in terms of alcohol (ROH) with a metal ion replacing the hydrogen atom in the hydroxyl group. Hydrolysis, metal alkoxide reacts readily with water, water attach to organic groups leading to the formation of hydroxyl groups. Furthermore, organic groups that are present in metal alkoxide can be completely replaced by water.

$$M(OR)_4 + H_2O \longrightarrow HO\text{–}M(OR)_3 + R\text{–}OH \quad (2.62)$$

$$M(OR)_4 + 4H_2O \longrightarrow M(OH)_4 + 4(R\text{–}OH) \quad (2.63)$$

Hydrolysis reaction rate can be increased by adding an acidic or basic catalyst. The chemical reaction of the formation of PTA synthesized by using metal alkoxide (Titanium tetraisopropoxide ($Ti(i\text{–}OC_3H_7)_4$)) as a precursor was introduced by following equations (Seok et al., 2010).

$$Ti(i\text{-}OC_3H_7)_4 + H_2O \longrightarrow Ti(OH)_4 + 4HO^iPr \quad (2.64)$$

$$Ti(OH)_4 + 4HO^iPr \xrightarrow{\text{Heating}} TiO_2.xH_2O \text{ (wet cake)} \quad (2.65)$$

$$TiO_2.xH_2O \text{ (wet cake)} + H_2O_2\text{aqueous} \xrightarrow{\text{Washing}} Ti(OH)_y(OOH)_z \text{ (solution)} \quad (2.66)$$

$$\text{aqueous } Ti(OH)_y(OOH)_z \text{ (solution)} \longrightarrow TiO_2 \quad (2.67)$$

In the case of inorganic salts such as $TiCl_4$ and $TiOSO_4$, the formation of TiO_2 can be qualitatively given by Equations (2.68)–(2.70) (Seok et al., 2010 and Ge et al., 2007).

$$TiCl_4 + H_2O \longrightarrow TiO(Cl)_2 + HCl \quad (2.68)$$

$$TiO(Cl)_2 + 4NH_4OH \longrightarrow TiO(OH)_2 + 4NH_4Cl \quad (2.69)$$

$$TiOSO_4 + 2NH_4OH \longrightarrow TiO(OH)_2 + (NH_4)_2SO_4 \quad (2.70)$$

The PTA solution can be obtained when $TiO(OH)_2$ is reacted with H_2O_2 and it can be also converted to TiO_2 by heating. Zhang et al. (2010c) suggested that Ti^{4+} hydrolyzes in the presence of H_2O_2 to from peroxotitanium complex that converts to dinuclear structure in an acidic solution. The dinuclear structures should be $Ti_2(O_2)_2(OH)_a(H_2O)_b$, $Ti_2(OOH)_2(OH)_a(H_2O)_b$ or $Ti_2(O_2)(OOH)(OH)_a(H2O)_b$, which depend on the concentration of the H_2O, H_2O_2 and pH. Peroxotitanium complex molecules develop binuclear molecules by using two peroxo groups to form an octahedron. Next, the OOH– and OH– groups of each binuclear molecule are connected to build linear chain via edge-sharing process, which leads to the formation of rutile lattice. In comparison with the formation of anatase phase, it is also depended on the reactions of OOH– and OH– but the face-sharing is a facility process to form anatase lattice at high pH because of the higher OH groups on peroxotitanium complex molecule. The formation of the TiO_2 anatase phase has been described. The white precipitate of $Ti(OH)_4$ is dissolved in H_2O_2 solution to form a homogeneous yellow aqueous PTA solution. The complex anion of titanium is basically considered as binuclear species, $Ti_2O_5(OH)_x^{(x-2)-}$ (x>2). When increased the temperature, binuclear complex species condenses to octahedral TiO_6 units in hydrated form and further crystalized to anatase TiO_2 via faces–haring condensation.